Spin-orbit torque driven chiral magnetization reversal in ultrathin nanostructures

N. Mikuszeit,[1,2,3,*] O. Boulle,[1,2,3] I. M. Miron,[1,2,3] K. Garello,[4] P. Gambardella,[4] G. Gaudin,[1,2,3] and L. D. Buda-Prejbeanu[1,2,3]

[1]*Université Grenoble Alpes, INAC-SPINTEC, F-38000 Grenoble, France*

[2]*CNRS, INAC-SPINTEC, F-38000 Grenoble, France*

[3]*CEA, INAC-SPINTEC, F-38000 Grenoble, France*

[4]*Department of Materials, ETH Zürich, Hönggerbergring 64, CH-8093 Zürich, Switzerland*

(Received 7 August 2015; published 26 October 2015)

We show that the spin-orbit torque induced magnetization switching in nanomagnets presenting Dzyaloshinskii-Moriya (DMI) interaction is governed by a chiral domain nucleation at the edges. The nucleation is induced by the DMI and the applied in-plane magnetic field followed by domain-wall propagation. Our micromagnetic simulations show that the dc switching current can be defined as the edge nucleation current, which decreases strongly with increasing amplitude of the DMI. This description allows us to build a simple analytical model to quantitatively predict the switching current. We find that domain nucleation occurs down to a lateral size of 25 nm, defined by the length scale of the DMI, beyond which the reversal mechanism approaches a macrospin behavior. The switching is deterministic and bipolar.

DOI: 10.1103/PhysRevB.92.144424 PACS number(s): 75.60.Jk, 85.70.Ay, 85.75.Dd

I. INTRODUCTION

The recent discovery that a current can switch the magnetization of a nanomagnet in ultrathin heavy-metal (HM)/ferromagnetic (FM) multilayers has opened a new path to manipulate magnetization at the nanoscale [1]. The switching arises from structural inversion asymmetry and high spin coupling, resulting in a spin current from the HM into the FM. This novel switching mechanism has led to an innovative magnetic memory concept, namely, the spin-orbit torque magnetic random access memory (MRAM) [1–3], which combines large endurance, low power, and fast switching and thus appears to be a possible nonvolatile alternative for cache memory applications. Recently, Garello *et al.* [4] demonstrated deterministic magnetization switching by spin-orbit torque (SOT) in ultrathin Pt/Co/AlO_x, as fast as 180 ps. These observations could not be explained within a simple macrospin approach, suggesting a magnetization reversal mechanism by domain nucleation and domain-wall (DW) propagation. The failure of the macrospin approach for quantitative description is also underlined by the predicted switching current density, which is nearly one order of magnitude larger than experimental ones [5–7]. Besides its fundamental importance, this lack of a proper quantitative modeling is an important issue for the design of logic and memory devices based on SOT switching, which have so far considered a macrospin description [8–11]. The missing ingredient is the presence of antisymmetric exchange interaction, i.e., Dzyaloshinskii-Moriya interaction (DMI). This exchange tends to form states of noncollinear magnetization, promoting a homochiral Néel DW [12–14]. In the Néel configuration, a maximal SOT is applied on the DW [13,15–17], which explains the large current-induced DW velocity observed experimentally [1,17]. Moreover, the DMI can result in significant magnetization tilting at the edges of magnetic structures, resulting, e.g., in asymmetric field-induced domain nucleation [18,19]. The influence of the DMI on the magnetization pattern during SOT switching was recently pointed out in micromagnetic simulation studies [20–22], whereas recent experimental work [23] explained the SOT switching mechanism by the expansion of a magnetic bubble.

Here, using micromagnetic simulations and analytic modeling, we show that the SOT-induced magnetization switching in the presence of DMI is governed by domain nucleation on one edge followed by propagation to the opposite edge. This reversal process allows us to explain the ultrafast deterministic switching observed experimentally. We systematically demonstrate that DMI leads to a large decrease of the switching current and of the switching time and thus strongly affects the reversal energy. On the basis of our micromagnetic simulations, we provide a simple analytical model, which allows us to quantitatively predict the SOT switching current in the presence of DMI. Finally, we address the evolution of the switching mechanism as the lateral dimension decreases, which is a key feature for the device scalability.

II. REVERSAL MECHANISM

The structures considered in this study are similar to the one used by Garello *et al.* [4]: a perpendicularly magnetized Co circular nanodot on top of a Pt stripe and capped with alumina. The DMI is included in the simulation using the expression of Ref. [13]. In addition to the standard micromagnetic energy density (which includes the exchange, magnetocrystalline anisotropy, Zeeman, and demagnetizing energies), the current injected in the Pt layer leads to two SOT terms in the the Landau-Lifshitz-Gilbert equation: the fieldlike $T_{\mathrm{FL}} \propto \vec{m} \times \vec{e}_y$ and the dampinglike $T_{\mathrm{DL}} \propto \vec{m} \times (\vec{m} \times \vec{e}_y)$, where $\vec{e}_y$ is the unit vector in the y direction (see [24] for additional details). If not state otherwise, the external applied field is $\mu_0 H_{\mathrm{app}} = -0.1$ T, and the material parameters are [25] the saturation magnetization $M_{\mathrm{S}} = 1090$ kA/m, the exchange constant $A_{\mathrm{ex}} = 1.0 \times 10^{-11}$ A/m, the perpendicular magnetic anisotropy constant $K_{\mathrm{u}} = 1248$ kJ/m^3, the DMI amplitude $D = 2$ mJ/m^2, the Gilbert damping parameter $\alpha = 0.5$, and the torques $T_{\mathrm{FL}}^0 = -0.05$ pTm^2/A and $T_{\mathrm{DL}}^0 = +0.1$ pTm^2/A.

*nikolai.mikuszeit@gmail.com

 ©2015 American Physical Society

The 3D micromagnetic simulations are performed using the solver MICRO3D [26] with a mesh size smaller than 1.5 nm. The initial magnetization state of the dot is the remanent state after saturation by a negative magnetic field ($-O_z$) as shown for 0 ps in Fig. 1(d). In the presence of an applied magnetic field $\vec{H}_{\rm app}$ in the x direction, magnetization dynamics is induced by a current pulse with a rise (and fall) time of 50 ps and variable width and amplitude. Typical simulation results of a 100-nm dot are presented in Fig. 1(a). Depending on the current amplitude, three regimes are identified:

(1) For $J_{\rm app} \leqslant 2.50 \times 10^{12}\,{\rm A/m^2}$ no magnetization switching is observed. The SOT leads to a slight tilting of the magnetization toward the plane of the dot, but the magnetization relaxes toward its initial equilibrium state after the pulse.

(2) At intermediate current values ($2.60 \times 10^{12}\,{\rm A/m^2} \leqslant J_{\rm app} \leqslant 3.70 \times 10^{12}\,{\rm A/m^2}$) magnetization reversal occurs. The time evolution of the magnetization pattern in the dot [see Fig. 1(d)] reveals that, in contrast to recent interpretations [23], the magnetization reversal occurs by domain nucleation shortly after the pulse injection (100 ps), followed by fast DW propagation. The nucleation always occurs on the left edge of the dot. Once nucleated, the DW propagates quickly through the dot and is expelled on the opposite edge. The switching time t_0, defined by $\langle m_z\rangle(t = t_0) = 0$, decreases as $J_{\rm app}$ increases; the increase of the slope of $\langle m_z\rangle(t)$ indicates that this is related to a faster DW propagation. As expected, the DW has a Néel configuration due to the large DMI. The simulation highlights that the DW nucleation occurs for all current values on the same edge in a deterministic way. Symmetrically, when reversing the sign of the current, the reversal from the up to the down state occurs on the opposite edge, i.e., the behavior is bipolar.

(3) For higher currents ($J_{\rm app} \geqslant 3.70 \times 10^{12}\,{\rm A/m^2}$) the motion of the DW becomes turbulent (oscillatory), and the coherence of the switching is destroyed.

The magnetization reversal scheme can be explained in a simplified manner by considering the combined effect of DMI, external magnetic field, and SOT but neglecting small variations of the demagnetizing field [27]. The DMI is too small to introduce a spin spiral but results in a magnetization canting at the dot edges [18,19,22]. The edge canting can be considered as effective field with spatial variation: on one side this field adds to the in-plane applied field, while it counteracts it on the other [see Fig. 1(b)]. This leads to an asymmetric tilting of the magnetization on both edges.

Upon current injection the dampinglike torque emerges. Its effect can be interpreted as a rotating magnetic field of the form $\vec{H}_{\rm DL} \propto J_{\rm app}\vec{m} \times \vec{e}_{\rm y}$ [see Fig. 1(c)]. This leads to a rotation of the magnetization towards the film plane on one side and away from the film plane on the other. Naturally, the current polarity is chosen such that the stronger tilted edge magnetization turns towards the film plane. Above a critical current an instability occurs, leading to domain nucleation and consecutive DW propagation. It is clear that the current $J_{\rm c}$, required to introduce the instability, reduces with increasing DMI. This behavior is seen in Fig. 2(a), where $J_{\rm c}$ tends to zero when $D \approx 3.8\,{\rm mJ/m^2}$. Moreover, for $J_{\rm app} > J_{\rm c}$ an increase of DMI decreases the switching time, as can be seen from Fig. 2(b). After expelling the DW on the opposite side, switching has occurred, and the more tilted edge appears on the opposite side. As the SOT rotates this side away from the film plane and is not sufficient to rotate the less tilted side into instability, the state is hence stable. It can easily be checked that this reversal scheme is in agreement with the hysteretic bipolar switching observed experimentally when sweeping $J_{\rm app}$ and $H_{\rm app}$ [1].

To understand these results better, we consider a simple analytical model which describes the reversal process in the presence of both DMI and SOT. Using a Lagrangian approach and following Pizzini *et al.* [19], the strategy is, eventually, similar to the Stoner-Wohlfarth approach in a single domain particle but using the energy functional per volume V

$$\frac{E(\theta)}{V} = -K_{\rm eff}\cos^2\theta - \mu_0 M_{\rm S} H_{\rm app}\sin\theta - M_{\rm S} J_{\rm app} T_{\rm DL}\theta, \qquad (1)$$

where the effect of the SOT is introduced by the last term [24]. The equilibrium magnetization angle in the center $\theta_{\rm c}$ is found by minimizing Eq. (1), while edge angle $\theta_{\rm e}$ is found by solving $[E(\theta_{\rm e}) - E(\theta_{\rm c})]/V = D^2/(4A)$ [24]. For small SOT and $\vec{H}_{\rm app}$, two stable solutions for $\theta_{\rm e}$ exist, corresponding to both sample edges. Above a threshold SOT one solution disappears, indicating that the magnetization on one edge is unstable, i.e., domain nucleation occurs. Using numerical methods, the critical current for nucleation $J_{\rm c}$ can be calculated easily as a function of D [see Fig. 2(a), black line]. Good agreement is obtained with micromagnetic simulation for a dot diameter $d = 100$ nm (circles). For D tending to zero, the nucleation current tends to the critical current predicted by the macrospin model $J_{\rm c} = 4.1 \times 10^{12}\,{\rm A/m^2}$ [6]. The absence of full quantitative agreement with micromagnetic simulation can be attributed to variations of the demagnetizing tensor and variations of the magnetization along the y direction due to the curvature of the dot. Better agreement is obtained when neglecting these effects in a quasi-one-dimensional simulation (square dots). Note that this nucleation current is actually the threshold current for quasi-dc current pulse.

III. CRITICAL CURRENT ANALYSIS

In the following, we discuss the dynamics of the magnetization switching. In Fig. 2(b) the switching time is shown as a function of $J_{\rm app} > J_{\rm c}$. With increasing $J_{\rm app}$ the switching time decreases rapidly as the DW velocity increases [16]. If D is reduced, the DW propagation is slower, resulting in a larger switching time. In the inset we show $J_{\rm app}$ versus $1/t_0$ for $D = 2\,{\rm mJ/m^2}$: a linear scaling is observed, in qualitative agreement with experiment [4].

Naturally, t_0 depends on the dot diameter. This is a key parameter for SOT applications. The evolution of the switching time vs the current density for varying dot sizes is shown in Fig. 2(c). When decreasing the diameter from 100 down to 50 nm, a shift to shorter switching times is observed, while a slightly higher onset current is found. Similar behavior is found when decreasing the size down to 30 nm and further down to 25 nm. It is, however, important to note that the latter two curves become identical for larger $J_{\rm app}$. Reducing the size down to 15 nm results in a dramatic increase of the threshold current density and deterministic switching is observed in only a narrow current density region. Overall, one has indications for three different size-dependent switching regimes. In the first regime the switching is covered by nucleation and

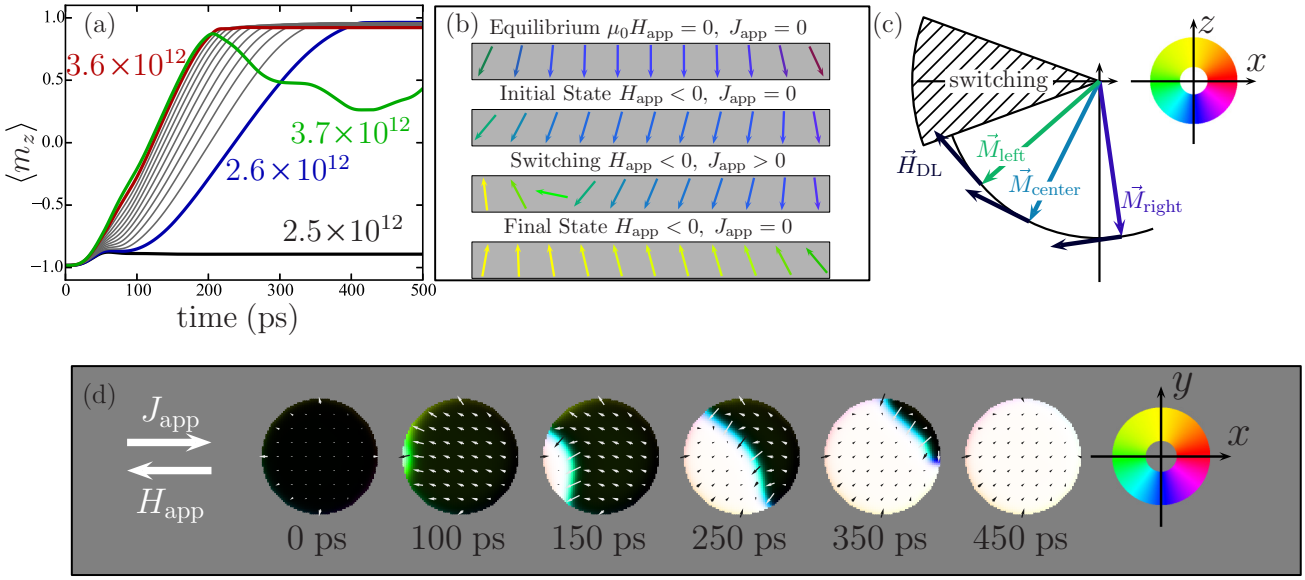

FIG. 1. (Color online) (a) Time evolution of the average out-of-plane magnetization for different applied current densities (variations in steps of 10^{11} A/m^2). The minimum current to trigger switching, i.e., the critical current, is highlighted in blue. The green curve indicates the threshold of turbulent behavior (see text). (b) Sketch of the magnetization configuration at different stages of the switching process. (c) Magnetization orientation in the center and at the left and right edges. The current-induced dampinglike torque (represented as effective field $\vec{H}_{\rm DL}$) can only drive the left edge magnetization into instability, resulting in a nucleation at the left edge. (d) Snapshots of the magnetization configuration showing the reversal from down (black) to up (white) via domain-wall nucleation and propagation under an externally applied field of $\mu_0 H = 0.1$ T and a current density of 2.6×10^{12} A/m^2.

propagation of a DW, and the decrease of t_0 is mainly caused by a reduced distance for the DW to travel. In the second regime the switching remains governed by DW propagation. The diameter, however, becomes comparable to approximately twice the value of $\xi = 2A/D \approx 10$ nm, the characteristic length scale on which canting of the edge magnetization is observed. In this situation the edge angle due to DMI differs from the ideal infinite case, and opposite edges are not completely independent anymore (see Ref. [24]). While this does not cause coherent rotation yet, it affects the DW motion. The coherent regime is reached at diameters in the range of the DW width $\Delta = \pi\sqrt{A/K_{\rm eff}} \approx 14$ nm. This explains the significant change in switching behavior for the 15-nm dot. Note that the switching current at this size is close to the one predicted by macrospin simulation (4.1×10^{12} A/m^2). It is worth mentioning that while the current density strongly increases with decreasing dot diameter, the current in the 3-nm-thick Pt stripe decreases almost linearly, as can be seen from Fig. 2(d). Therefore, the device exhibits favorable scaling behavior and, assuming a 1-kΩ resistance for the addressing transistor of a 30-nm dot, switching in about 300 ps, needs only 20 fJ for one switching event, which is significantly smaller than the energy for perpendicular spin-transfer torque devices [28].

Naturally, the threshold current and switching time depend on several intrinsic as well as extrinsic parameters. We have studied in detail the influence of the applied field, the damping constant, the strength of the fieldlike torque, and temperature. The results are shown in Fig. 3. Variations in these parameters lead to quantitative changes of the nucleation current as well as the switching time. In all cases this is

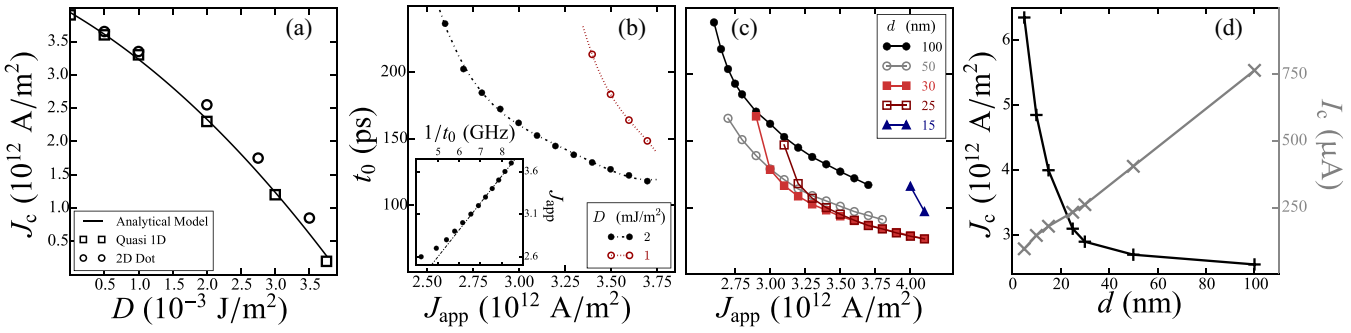

FIG. 2. (Color online) (a) Critical current for destabilizing the system as a function of the DMI strength. (b) The relation between the critical current and the switching time t_0 for two different values of DMI. The inset shows the data for $D = 2$ mJ/m^2 but in a transformed coordinate system $J_{\rm app}$ vs t_0^{-1}. (c) The switching time vs current for different dot diameters. (d) Critical current and current density for different dot sizes. The calculation of the current assumes a 3-nm-thick Pt line.

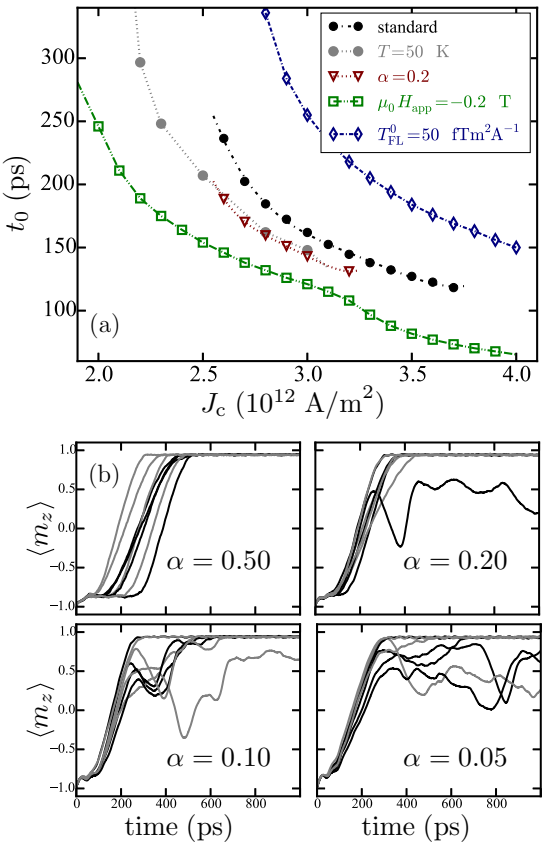

FIG. 3. (Color online) (a) Switching time as a function of the applied current density, varying intrinsic and extrinsic parameters. For the temperature case, the average t_0 is plotted. The single event switching time is defined as before, while the average t_0 is defined as the time when the probability of stochastic switching reaches 90%. (b) Several switching graphs $\langle m_z \rangle(t)$ for varying damping at $T = 50$ K and $J_{app} = 2.6 \times 10^{12}$ A/m^2. For fixed α variations are only due to temperature fluctuations.

attributed mainly to changes in DW velocity; lower damping increases the wall velocity and so does an in-plane field, as it promotes and stabilizes a Néel-type wall. A negative fieldlike torque also stabilizes the DW, while a positive one destabilizes it, therefore increasing the switching time. The edge nucleation/DW propagation mechanism, however, is not affected. Most importantly, Fig. 3(a) shows that the mechanism of switching by nucleation and propagation is very robust against fluctuations due to temperature (see Ref. [24] for more details). The temperature fluctuations strongly decrease the threshold current [Fig. 3(b)]. Temperature effectively lowers the nucleation barrier, such that nucleation times get shorter and, consequently, the whole switching becomes faster. It has to be pointed out that the nucleation still takes place at the same position on the dot edge, and the overall process remains bipolar with respect to field and current reversal. This temperature robustness, however, strongly relies on the large damping, as can be seen from Fig. 3(b). With decreasing α an increasing tendency of oscillations is observed, such that deterministic switching cannot be guaranteed [6].

IV. CONCLUSIONS

To conclude, we have studied the current-induced magnetization switching of a nanomagnet by spin-orbit torques in the presence of Dzyaloshinskii-Moriya interaction. The critical switching current strongly decreases with increasing amplitude of DMI, and we provide a simple analytical model for this dependency. This switching mechanism via chiral domain nucleation explains the deterministic switching observed experimentally in ultrathin Pt/Co/AlO$_x$ even for subnanosecond pulses. The switching is mainly introduced by the dampinglike torque, but the fieldlike torque cannot be neglected as it strongly influences the switching time. Our systematic study shows a change in the reversal mechanism below diameters of 30 nm, while the switching remains deterministic and bipolar. However, at 0 K the operational window for current densities decreases with decreasing dot diameter. The influence of temperature on this technologically important limit will be investigated in the future. Most importantly, current scalability is maintained. Confirming the potential of SOT-MRAM for scalable fast nonvolatile memory application, our results will help in the design of devices based on this technology.

ACKNOWLEDGMENTS

This work was funded by the spOt project (318144) of the EC under the Seventh Framework Programme.

[1] I. Miron, K. Garello, G. Gaudin, P.-J. Zermatten, M. V. Costache, S. Auffret, S. Bandiera, B. Rodmacq, A. Schuhl, and P. Gambardella, Nature (London) **476**, 189 (2011).
[2] L. Liu, C.-F. Pai, Y. Li, H. W. Tseng, D. C. Ralph, and R. A. Buhrman, Science **336**, 555 (2012).
[3] M. Cubukcu, O. Boulle, M. Drouard, K. Garello, C. Avci, I. Miron, J. Langer, B. Ocker, P. Gambardella, and G. Gaudin, Appl. Phys. Lett. **104**, 042406 (2014).
[4] K. Garello, C. Avci, I. Miron, M. Baumgartner, A. Ghosh, S. Auffret, O. Boulle, G. Gaudin, and P. Gambardella, Appl. Phys. Lett. **105**, 212402 (2014).
[5] L. Liu, O. J. Lee, T. J. Gudmundsen, D. C. Ralph, and R. A. Buhrman, Phys. Rev. Lett. **109**, 096602 (2012).
[6] K.-S. Lee, S.-W. Lee, B.-C. Min, and K.-J. Lee, Appl. Phys. Lett. **102**, 112410 (2013).
[7] K.-S. Lee, S.-W. Lee, B.-C. Min, and K.-J. Lee, Appl. Phys. Lett. **104**, 072413 (2014).
[8] Y. Kim, X. Fong, K.-W. Kwon, M.-C. Chen, and K. Roy, IEEE Trans. Electron Devices **62**, 561 (2015).
[9] K. Jabeur, G. Di Pendina, and G. Prenat, Electron. Lett. **50**, 585 (2014).
[10] K. Jabeur, G. Di Pendina, G. Prenat, L. D. Buda-Prejbeanu, and B. Dieny, IEEE Trans. Magn. **50**, 1 (2014).
[11] Z. Wang, W. Zhao, E. Deng, J.-O. Klein, and C. Chappert, J. Phys. D **48**, 065001 (2015).

[12] G. Chen, J. Zhu, A. Quesada, J. Li, A. T. N'Diaye, Y. Huo, T. P. Ma, Y. Chen, H. Y. Kwon, C. Won, Z. Q. Qiu, A. K. Schmid, and Y. Z. Wu, Phys. Rev. Lett. **110**, 177204 (2013).
[13] A. Thiaville, S. Rohart, E. Jué, V. Cros, and A. Fert, Eur. Phys. Lett. **100**, 57002 (2012).
[14] J.-P. Tetienne, T. Hingant, L. J. Martínez, S. Rohart, A. Thiaville, L. H. Diez, K. Garcia, J.-P. Adam, J.-V. Kim, J.-F. Roch, I. M. Miron, G. Gaudin, L. Vila, B. Ocker, D. Ravelosona, and V. Jacques, Nat. Commun. **6**, 6733 (2015).
[15] S. Emori, U. Bauer, S.-M. Ahn, E. Martinez, and G. S. D. Beach, Nat. Mater. **12**, 611 (2013).
[16] O. Boulle, S. Rohart, L. D. Buda-Prejbeanu, E. Jué, I. M. Miron, S. Pizzini, J. Vogel, G. Gaudin, and A. Thiaville, Phys. Rev. Lett. **111**, 217203 (2013).
[17] K.-S. Ryu, L. Thomas, S.-H. Yang, and S. Parkin, Nat. Nanotechnol. **8**, 527 (2013).
[18] S. Rohart and A. Thiaville, Phys. Rev. B **88**, 184422 (2013).
[19] S. Pizzini, J. Vogel, S. Rohart, L. D. Buda-Prejbeanu, E. Jué, O. Boulle, I. M. Miron, C. K. Safeer, S. Auffret, G. Gaudin, and A. Thiaville, Phys. Rev. Lett. **113**, 047203 (2014).
[20] N. Perez, E. Martinez, L. Torres, S.-H. Woo, S. Emori, and G. Beach, Appl. Phys. Lett. **104**, 092403 (2014).
[21] G. Finocchio, M. Carpentieri, E. Martinez, and B. Azzerboni, Appl. Phys. Lett. **102**, 212410 (2013).
[22] E. Martinez, L. Torres, N. Perez, M. A. Hernandez, V. Raposo, and S. Moretti, Sci. Rep. **5**, 10156 (2015).
[23] O.-J. Lee, L.-Q. Liu, C.-F. Pai, Y. Li, H.-W. Tseng, P. G. Gowtham, J. P. Park, D. C. Ralph, and R. A. Buhrman, Phys. Rev. B **89**, 024418 (2014).
[24] See Supplemental Material at http://link.aps.org/supplemental/10.1103/PhysRevB.92.144424 for details on the equation of motion, a detailed elaboration of the Lagrange formalism and the resulting analytical model, as well as additional data on size and temperature dependence.
[25] K. Garello, I. Miron, C. Avci, F. Freimuth, Y. Mokrousov, S. Blügel, S. Auffret, O. Boulle, G. Gaudin, and P. Gambardella, Nat. Nanotechnol. **8**, 587 (2013).
[26] L. D. Buda, I. Prejbeanu, U. Ebels, and K. Ounadjela, Comput. Mater. Sci. **24**, 181 (2002).
[27] S. Meckler, O. Pietzsch, N. Mikuszeit, and R. Wiesendanger, Phys. Rev. B **85**, 024420 (2012).
[28] H. Liu, D. Bedau, J. Z. Sun, S. Mangin, E. E. Fullerton, J. A. Katine, and A. D. Kent, J. Magn. Magn. Mater. **358-359**, 233 (2014).